

# A Monte-Carlo study of sub-keV electron transport in water: the influence of the condensed phase

D. Emfietzoglou <sup>a,f,\*</sup>, G. Papamichael <sup>b</sup>, I. Androulidakis <sup>c</sup>, K. Karava <sup>a</sup>,  
K. Kostarelos <sup>d</sup>, A. Pathak <sup>e</sup>, M. Moscovitch <sup>f</sup>

<sup>a</sup> Department of Medical Physics, University of Ioannina Medical School, Ioannina 451 10, Greece

<sup>b</sup> Department of Mechanical Engineering, National Technical University of Athens, Athens 157 10, Greece

<sup>c</sup> Department of Physics, University of Ioannina, Ioannina 451 10, Greece

<sup>d</sup> Department of Chemistry, Imperial College London, South Kensington Campus, SW7 2AZ, UK

<sup>e</sup> School of Physics, University of Hyderabad, Hyderabad 500 046, India

<sup>f</sup> Department of Radiation Medicine, Georgetown University Medical Center, Washington DC 20007, USA

## Abstract

We explore the influence of condensed phase in various single-collision and slowing-down distributions of low-energy (sub-keV) electron tracks in water (i.e. vapor versus liquid phase at the same density). A unified methodology for both phases has been developed and implemented in our Monte-Carlo code based on elements of the Born and Bethe theories which are used to establish cross-sections for inelastic electronic scattering, the main mechanism of energy loss in the present study. The linear dielectric response theory was used for the valence shells of the liquid phase implemented by Born-corrections at low energies. By using experimental optical data as input, various many-body effects, such as, polarisation, collective excitations and correlation, are, for the most part, automatically accounted for. Monte-Carlo calculations of the spatial pattern of energy distribution, as well as, the clustering properties of collision events in full slowing-down electron tracks have been performed for both the vapor and liquid phases of water. The degree in which various model assumptions pertaining to the condensed-phase influence the above distributions is examined.

© 2004 Elsevier B.V. All rights reserved.

**Keywords:** Monte-Carlo; Electron transport; Condensed-phase; Water

## 1. Introduction

Electrons with kinetic energies in the sub-keV range, named here low-energy electrons (LEEs), play an important role in the mechanism

\* Corresponding author. Tel.: +30 26510 97741; fax: +30 26510 97854.

E-mail address: [demfietz@cc.uoi.gr](mailto:demfietz@cc.uoi.gr) (D. Emfietzoglou).

of radiation action in matter by almost any sufficiently energetic particle beam [1]. The reason being that LEEs are abundantly produced during the slowing-down process and the dissipation of their energy is confined within sub-micron volumes. This spatial scale is often associated with important functional units in both biological systems and electronic devices. For example, cancer induction and cell-kill by radiation is supposed to be triggered by molecular events in the cell nucleus (few  $\mu\text{m}$ ) associated with clustered damage in the DNA double-helix (few nm) and/or chromatin-size targets (10–100 nm) [2]. On the other hand, single-event-upsets (SEUs) in micro-electronic-cells are also associated with ionisation events in a submicron node of the device [3]. Due to the close proximity (nm-separation) of successive ionisation events in LEE tracks, their characteristic spatial pattern of interactions and energy deposition is by far more efficient compared to higher energy electrons in inducing clustered damage [4].

The study of LEEs, however, poses serious challenges due to the gradual failure of classical (binary) interaction models in the sub-keV range. The details of the electronic structure now become critical, giving rise to many-body effects in the scattering process. With respect to biological matter and the modelling of cellular radiation action, water has been traditionally the material of choice, being a realistic approximation of the cellular medium. The degree in which, however, condensed-phase effects (i.e. vapor versus liquid phase at the same density) are important to modeling LEE tracks in water has been debated since the mid-70s; for a review see [5]. At the core of this debate lies the availability of well-established experimental cross-section data for the vapor phase, in sharp contrast to the limited information on the scattering properties of the liquid phase. Thus, vapor-based Monte-Carlo (MC) codes are generally considered more reliable than liquid-based MC codes, although the latter are supposed to be a more realistic approximation of the liquid-like cellular environment. However, the use of vapor data extrapolated linearly to unit density (i.e. the so-called gas-phase approximation of liquid water) neglects any non-linear density effects

in the scattering process. The latter are known to be gradually more pronounced at low energies and, therefore, might be particularly important in modeling LEE tracks [6–8].

In the present study, we explore the influence of condensed phase (i.e. vapor versus liquid phase at the same density) in various single-collision and slowing-down distributions of sub-keV electron tracks in water. A unified methodology for both phases has been developed based on elements of the Born and Bethe theories which are used to establish inelastic cross-sections for energy loss. The linear dielectric response theory was used for the valence shells of the liquid phase together with Born-corrections at low energies. The methodology has been implemented in our Monte-Carlo code, MC4 [9], which performs full slowing-down simulation of electrons in an event-by-event mode and used for various track-structure calculations. Thereafter, the vapor-based version of the code will be denoted as MC4V, whereas, the liquid-based version as MC4L. All vapor results have been normalised to unit density.

## 2. Inelastic models

The first Born approximation (FBA) provides a suitable starting point for the description of the inelastic scattering process. The important result of this approximation is the factorisation of the doubly-differential inelastic cross-section into a kinematic (projectile-dependent) and a dynamic (target-dependent) factor as follows [10]:

$$\frac{d^2\Sigma^{(1)}}{dE dQ} = \frac{8\pi\alpha_0^2 R^2 N Z}{T} \times \frac{S(q, E)}{Q^2}, \quad (1)$$

where  $E$  is the energy-transfer,  $Q = q^2/2m$  with  $q$  the momentum-transfer and  $m$  the electron rest mass,  $T$  is kinetic energy of the incident electron,  $\alpha_0$  is the Bohr radius,  $R$  is the Rydberg constant,  $N$  is the molecular density,  $Z$  is the atomic number and  $S(q, E)$  is the inelastic form-factor. According to common practice for condensed targets we use the macroscopic cross-section,  $\Sigma$ , also called the inverse mean-free-path, IMFP.

Eq. (1) may be directly used for modelling the energy loss and angular deflection (i.e. momentum transfer) in an inelastic collision. In view, however, of the prominence of momentum transfer in elastic scattering, it is advantageous for an MC simulation to model the  $E$ -dependence directly from Bethe's asymptotic expansion. In accordance with the restrictions of the FBA, we keep only the first-order term and write the singly-differential cross-section as follows:

$$\frac{d\Sigma^{(1)}}{dE} = [A(E) \ln(T/R) + B(E)]T^{-1}, \quad (2)$$

where  $T = 1/2mu^2$  ( $m$ : electron mass) and  $A(E), B(E)$  are target properties directly related to the form-factor. In particular, the  $A(E)$  depends on the optical-limit,  $S(q = 0, E)$ , whereas the  $B(E)$  relates to the full  $q$ -dependence of  $S(q, E)$ . The difference between our vapor and liquid inelastic models lie solely in these two target-parameters, which have to be determined separately for the two phases of water. Since any phase effects would be limited to the valence shells, the core-shell of water (i.e. the oxygen K-shell) is treated within the binary-encounter-approximation with exchange included [11].

### 2.1. Liquid phase

For the liquid phase, we take advantage of the following relationship between the form-factor and the loss-function:

$$S(q, E) = \frac{2}{\pi} \frac{Q}{E_p^2} Z \operatorname{Im} \left[ -\frac{1}{\varepsilon(q, E)} \right], \quad (3)$$

where  $\varepsilon(q, E) = \varepsilon_1 + i\varepsilon_2$  is the complex dielectric-response function,  $E_p$  is the plasma energy of liquid water (21.6 eV), and  $\operatorname{Im}(-1/\varepsilon)$  is the loss-function. It may then be shown that

$$A(E) = \frac{1}{2\pi\alpha_0} \operatorname{Im} \left[ \frac{-1}{\varepsilon(q = 0, E)} \right]. \quad (4)$$

Importantly the optical-loss-function in Eq. (4) may be determined from optical data by using the following relationship:

$$\operatorname{Im} \left[ \frac{-1}{\varepsilon(0, E)} \right] = \frac{2nk}{(n^2 - k^2)^2 + (2nk)^2}, \quad (5)$$

where  $n = n(E)$  and  $k = k(E)$  are the real and imaginary parts of the index of refraction, respectively, which have been experimentally measured for liquid water. A modified Drude expansion model has been used to analytically represent the optical data consistent with the appropriate sum-rules. The following formula pertains to this model:

$$\varepsilon(0, E) = 1 + E_p^2 \sum_j \frac{f_j}{E_j^2 - E^2 - i\gamma_j E}, \quad (6)$$

where the  $E_j$ ,  $f_j$  and  $\gamma_j$  are the adjustable model parameters found from the analytic representation of the optical data. The details of this procedure may be found in [12].

On the other hand, the  $B(E)$  parameter formally relates to the  $q$ -dependence of the form-factor. We have examined various dispersion ( $q > 0$ ) models for calculating proton [13] and electron [14] inelastic characteristics in liquid water. Here, we use the extended-Drude model as first suggested by Ritchie et al. [15]. The loss-function may then be calculated from

$$\operatorname{Im} \left[ \frac{-1}{\varepsilon(q, E)} \right] = \frac{\varepsilon_2(q, E)}{\varepsilon_1^2(q, E) + \varepsilon_2^2(q, E)}, \quad (7)$$

where the  $\varepsilon_1 = \operatorname{Re}[\varepsilon(q, E)]$  and  $\varepsilon_2 = \operatorname{Im}[\varepsilon(q, E)]$  are now found from Eq. (6) under the substitution  $E_j(q) = E_j + q^2/2m$ , in accordance with the impulse approximation (restricted to the continuum), and  $f_j = f_j(q)$ , in accordance with an empirical generalised-oscillator-strength formula. We may then determine the  $B(E)$  by numerically integrating Eq. (1) and solving Eq. (2). For the continuum, we also account for the binary limit at large  $E$  by means of the binary-encounter-approximation. The details of this procedure are discussed in [16].

Perturbation corrections were included by means of a second-order term:

$$\frac{d\Sigma^{(2)}}{dE} = -\frac{2}{\pi\alpha_0 T} \operatorname{Im} \left[ \frac{-1}{\varepsilon(0, E)} \right] L(E). \quad (8)$$

Eq. (8) was based on a classical impact-parameter perturbation calculation where the  $L(E)$  function depends on the cut-off distance that distinguishes between close and distant collisions in the calculation [17]. This function, however, becomes negative below about 100 eV. Therefore, a

simple Coulomb-field correction [18] was adopted at lower energies which results in the substitution of  $T$  by  $T + I_j + U_j$ , where  $I_j$  and  $U_j$  are the binding and kinetic energy, respectively, of an electron at the  $j$ th orbital. An exchange correction term was applied to the continuum by analogy to the Mott formula:

$$\frac{d\Sigma_j^{(ex)}(W, T)}{dW} = \frac{d\tilde{\Sigma}_j(T - W - I_j, T)}{dW} - \left[ \frac{d\tilde{\Sigma}_j(W, T)}{dW} \times \frac{d\tilde{\Sigma}_j(T - W - I_j, T)}{dW} \right]^{1/2}, \quad (9)$$

where  $W$  is the kinetic energy of the secondary electron ( $W = E - I_j$ ), and

$$\frac{d\tilde{\Sigma}_j}{dW} = \frac{d\Sigma_j^{(1)}}{dW} + \frac{d\Sigma_j^{(2)}}{dW}. \quad (10)$$

## 2.2. Vapor phase

For the vapor phase, we use the relationship between the form-factor and the oscillator-strength of the molecule:

$$S(q, E) = \frac{Q}{E} \frac{df(q, E)}{dE}, \quad (11)$$

where  $df(q, E)/dE$  is the generalised-oscillator-strength (GOS). The  $A(E)$  may then be found from

$$A(E) = 4\pi\alpha_0^2 R^2 N \frac{df(q=0, E)}{EdE}, \quad (12)$$

where  $df(0, E)/dE$  is the optical-oscillator-strength (OOS) which may be obtained from

$$\frac{df(0, E)}{dE} = (4\pi^2\alpha_0^2 R)^{-1} \sigma_{ph}, \quad (13)$$

where  $\alpha$  is the fine structure constant and  $\sigma_{ph}$  the photo-absorption cross-section. The analytic determination of the OOS for the water molecule based on experimental  $\sigma_{ph}$  data has been given in [19].

The  $B(E)$  for the vapor is found directly from Eq. (2) by using the experimental inelastic cross-section data at the limited incident energies available. However, since, formally, the  $B(E)$  is independent of  $T$ , it may then be used at any incident energy. Similar to the liquid case, the binary-encounter-

approximation (with an exchange correction) was used as an asymptotic limit of Eq. (2) for the continuum. Any further low-energy Born corrections are automatically incorporated in the empirical derivation of  $B(E)$ , since the available cross-section data for the vapor go down to a few tens of eV. The procedure is discussed in more detail in [19].

## 3. Angular deflections

Data on the angular distribution of electrons in liquid water following an elastic or inelastic collision do not exist. As a result, and in view of the difficulties associated with the theoretical treatment of this problem, a methodology applied earlier to the vapor phase has been adopted here for both phases. In view of other uncertainties, this is a reasonable approximation. In summary, the screened-Rutherford formula with Moliere's screening parameter has been used for the total elastic, as well as, for the differential above 200 eV. At lower energies empirical distributions were used [20]. The angular distributions of the scattered and secondary electrons after ionisation were obtained based on the kinematics of binary collisions and the data of Opal and co-workers as described in [21].

## 4. Results

In Figs. 1(a) and (b) we present secondary electron spectra for electron ionisation collisions in vapor and liquid water for two characteristic incident energies, namely, for 1 and 0.1 keV. The liquid results have been calculated by the FBA (a first-order perturbation theory), the FBA supplemented by a second-order term plus an exchange correction, as well as, by the simple Mott formula modified by the binding energies of liquid water. It may first be seen that corrections to the FBA are unimportant at 1 keV (the two plots are indistinguishable in Fig. 1(a)), becoming of the order of 50% at the peak ( $W \approx 10$  eV) of the 0.1 keV distribution (Fig. 1(b)). It is also evident that the vapor spectra are notably different from the liquid spectra. At both energies the liquid spectra are

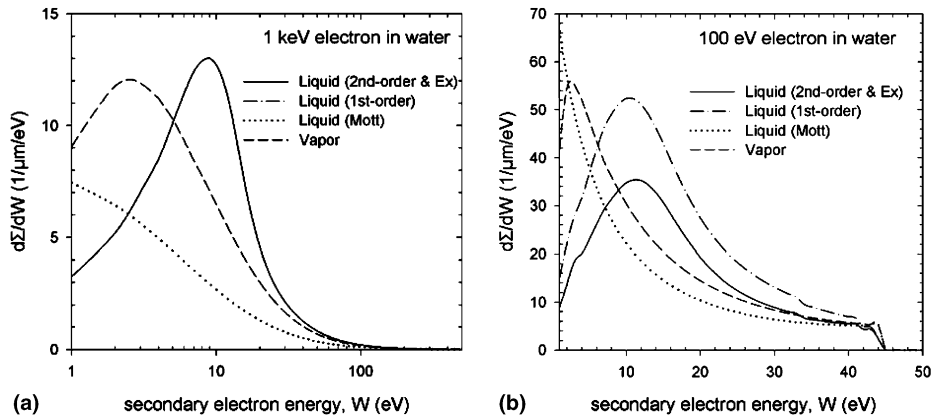


Fig. 1. Secondary electron spectra for electron impact in the two phases of water calculated by various inelastic models: (a) 1 keV electron impact; (b) 0.1 keV electron impact.

harder; the most probable secondary energy is about 10 eV for the liquid whereas it is only 2–3 eV for the vapor. This is due to an up-ward shift of the oscillator-strength in the condensed phase resulting from inter-molecular bonding [6]. The Mott calculations fail to reproduce the proper shape of the secondary spectra, especially at the low-energy range where the binary approximation fails. As expected, all distributions come together at high secondary energies where the details of electronic structure become gradually less important.

In Fig. 2 we present the inelastic IMFP from 10 keV down to threshold. Regarding phase-effects the following conclusions follow: (i) Differences between the two phases become noticeable below 1 keV, since the binary character prevails at higher impact energies; (ii) The vapor IMFP is by a factor of 1.4 higher than the liquid at 100 eV, due to screening effects in the condensed phase; (iii) The vapor IMFP peaks at lower impact energies ( $\sim 70$  eV) compared to the liquid ( $\sim 120$  eV), due to the upward shift of the oscillator-strength in the condensed phase; (iv) The correction terms to the FBA appear to be important below 1 keV, especially since the magnitude of the correction is of the same order as the vapor–liquid difference. Nevertheless, the screening and upward shift in the liquid is still evident in the FBA results. As expected, the Mott-calculated IMFP is way off throughout most of the depicted energy range, a

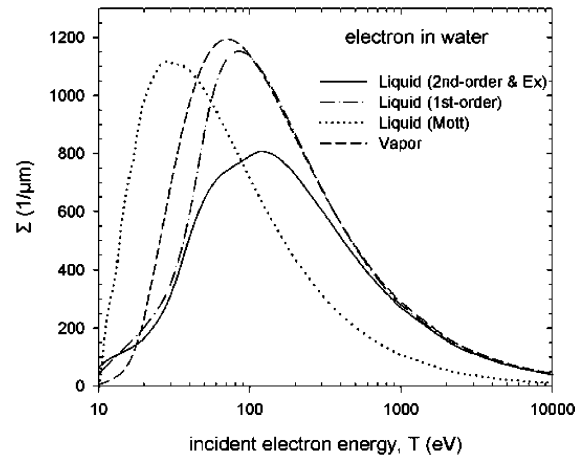


Fig. 2. Electron inelastic inverse-mean-free-path (IMFP) for the two phases of water calculated by various inelastic models.

direct consequence of the failure of the binary approximation in the low-energy range.

In Fig. 3 the dependence of the mean energy loss,  $\langle E_{\text{loss}} \rangle$  per collision on incident electron energy is shown. In relation to previous discussion, it may be clearly seen in this figure that the harder collision spectrum in the liquid phase results in a larger mean value than in the vapor by about 5 eV. A binary approximation, on the other hand, results in even larger differences as the Mott results indicate.

In the following figures we present and compare MC calculations from full slowing-down electron

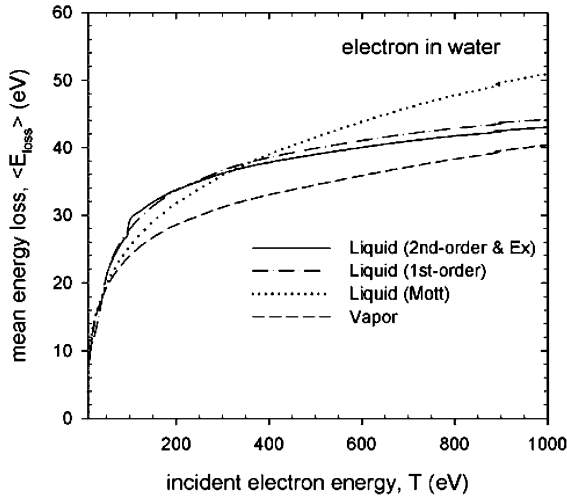


Fig. 3. Average energy loss as a function of incident energy for electron inelastic impact in the two phases of water calculated by various inelastic models.

tracks (followed down to 1 Ry) from the MC4V and MC4L versions.

Figs. 4(a) and (b) present distributions of absorbed energy (per track) in spherical shells at 1 nm radial intervals from the point of origin of monoenergetic electron sources of 0.1, and 1 keV initial energies. To obtain reasonable statistics, the results are averaged over 1000 and 10000 electron tracks, respectively. Although the liquid distributions do appear to have a slightly smaller spread-out pattern (rise higher and peak earlier)

than the vapor ones at the 1 keV energies, the effect is much smaller than previously considered [22]. In particular, these results reveal that the screening effect, which is responsible for larger MFPs in the liquid, is almost equally compensated by the effect of the hardening of the liquid spectrum (larger  $\langle E_{\text{loss}} \rangle$ ), which acts in the opposite direction resulting in the dissipation of energy closer to the origin. Interestingly, this pattern is reversed at very low energies (the 100 eV case) where the screening effect seems to be more important than the hardening effect, i.e. it is the MFP and not the  $\langle E_{\text{loss}} \rangle$  which governs the distribution. This is reasonable, in view of the much smaller number of collisions during slowing-down at this incident energy. The above arguments are further supported by the behaviour of the FBA-based distributions. Here, the effect of screening is minimal (the MFP is very close to the vapor), whereas the hardening is still in effect. As a result, the 100 eV distribution is very close to the vapor, whereas the higher energy distributions show a smaller spread-out pattern. The Mott-based distributions may be explained by the same arguments.

Although the pattern of energy deposition as presented, for example, in Fig. 4, provides important information on track-structure characteristics, biological damage is largely the result of clustering of events in critical cellular structures. One of the most basic clustering characteristic is the probability distribution of distances between two inelastic

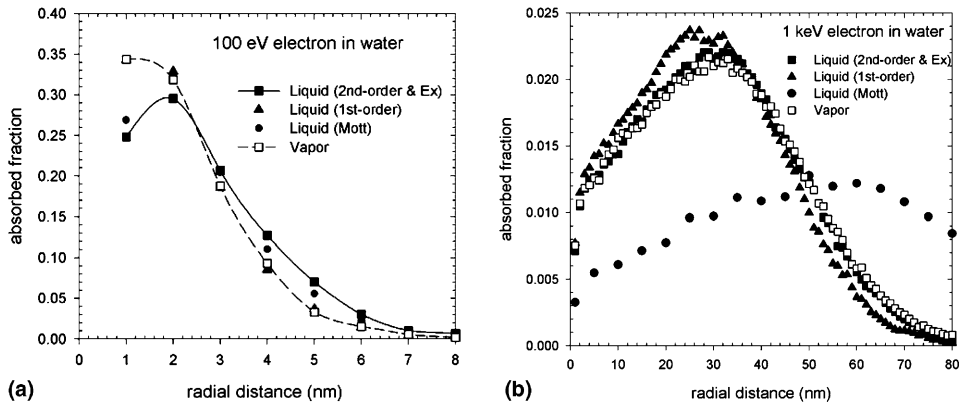


Fig. 4. Monte-Carlo calculated radial distribution of absorbed fraction in spherical shells of 1 nm intervals centred at the electron-track origin in the two phases of water. The initial electron energy was: (a) 0.1 keV (the two lines are to guide the eye), (b) 1 keV.

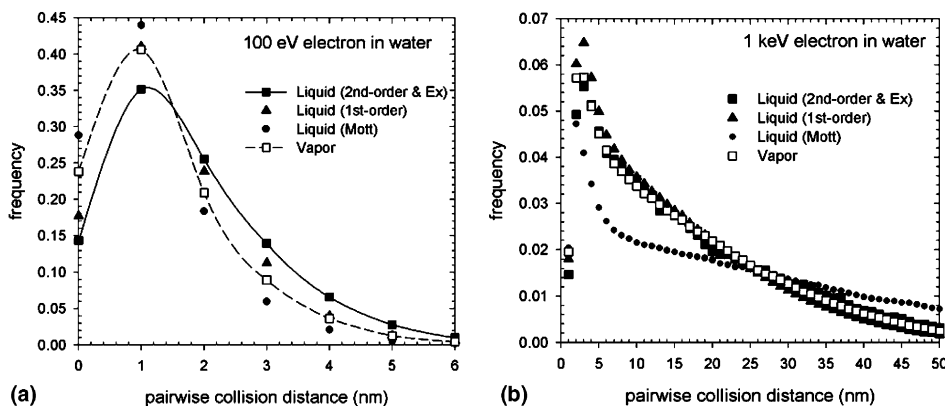


Fig. 5. Monte-Carlo calculated frequency distribution of distances between inelastic collisions in full slowing-down electron tracks in the two phases of water. The initial electron energy was: (a) 0.1 keV (the two lines are to guide the eye), (b) 1 keV.

collisions. Such distribution provides also important information for the subsequent chemistry. In Figs. 5(a) and (b) we present such distributions at three different initial electron energies calculated on the basis of the same inelastic models as in Fig. 4. At all energies, the distribution peaks at about 1–3 nm distances which is of particular significance considering that 2 nm is the diameter of the DNA double helix. As the electron increases, the tail of the distribution increases due to the larger MFPS involved. The vapor distributions peak at the same distances with the liquid (the corrected-FBA results) but higher due to the larger IMFP in the vapor phase (see Fig. 2) which results in smaller distances between successive collisions. The reason that the FBA distributions of the liquid peak even higher than the vapor, although the respective IMFPs are somewhat lower (see Fig. 2), is due to the more efficient dissipation of energy in the liquid, which, in turn, is the result of the higher  $\langle E_{\text{loss}} \rangle$ .

### Acknowledgements

This research is sponsored by the U.S. Department of Energy under contract No. DE-AC05-96OR22464 (NN-22) program with UT-BATTELLE, and by Grant 62/1405 registered with the University of Ioannina Committee of Research.

### References

- [1] H. Paretzke, Kinetics of Non-Homogeneous Processes, Wiley, New York, 1987, p. 89.
- [2] H. Nikjoo, P. O'Neill, W.E. Wilson, D.T. Goodhead, Radiat. Res. 156 (2001) 577.
- [3] M.A. Xapsos, Nucl. Instr. and Meth. B 184 (2001) 113.
- [4] H. Nikjoo, D.T. Goodhead, Phys. Med. Biol. 36 (1991) 229.
- [5] IAEA, Atomic and molecular data for radiation therapy and related research, Vienna, 1995.
- [6] J.E. Turner, H.G. Paretzke, R.N. Hamm, H.A. Wright, R.H. Ritchie, Radiat. Res. 92 (1982) 47.
- [7] H.G. Paretzke, J.E. Turner, R.N. Hamm, H.A. Wright, R.H. Ritchie, J. Chem. Physics 84 (1986) 3182.
- [8] H. Nikjoo, M. Terrisol, R.N. Hamm, J.E. Turner, S. Uehara, H.G. Paretzke, D.T. Goodhead, Radiat. Prot. Dosim. 52 (1994) 165.
- [9] D. Emfietzoglou, G. Papamichael, M. Moscovitch, J. Phys. D 33 (2000) 932.
- [10] M. Inokuti, Rev. Mod. Phys. 43 (1971) 297.
- [11] ICRU Report 55, Bethesda MD, 1996.
- [12] D. Emfietzoglou, M. Moscovitch, Nucl. Instr. and Meth. B 193 (2002) 71.
- [13] D. Emfietzoglou, M. Moscovitch, A. Pathak, Nucl. Instr. and Meth. B 212 (2003) 101.
- [14] D. Emfietzoglou, Radiat. Phys. Chem. 66 (2003) 373.
- [15] R.H. Ritchie, A. Howie, Philos. Mag. 36 (1977) 463.
- [16] D. Emfietzoglou, K. Karava, G. Papamichael, M. Moscovitch, Phys. Med. Biol. 48 (2003) 2355.
- [17] J.C. Ashley, J. Phys.: Condens. Matter 3 (1991) 2741.
- [18] F. Salvat, J.D. Martinez, R. Mayol, J. Parellada, J. Phys. D 18 (1985) 299.
- [19] D. Emfietzoglou, G. Papamichael, K. Kostarelos, M. Moscovitch, Phys. Med. Biol. 45 (2000) 3171.

- [20] D.J. Brenner, M. Zaider, *Phys. Med. Biol.* 29 (1983) 43.
- [21] B. Grosswendt, E. Waibel, *Nucl. Instr. and Meth.* 155 (1978) 145.
- [22] H. Nikjoo, S. Uehara, *Computational Approaches in Molecular Radiation Biology*, Plenum Press, New York, 1994, p. 167.